Analysis of a hybrid LFG-Concentrated Solar Power concept for landfill energy recover

Apresentado ao Journal of Cleaner Production - 2020

Mario B. Siqueira[a,*] and Arthur Monteiro Filho[b]
[a] Dept Mechanical Engineering, University of Brasilia
[b] Dept. Mechanical Engineering, Federal Institute of Espirito Santo
[*] Corresponding author
Email addresses mariosiqueira@unb.br (M. B. Siqueira)

ABSTRACT

In the present study, new approaches for Landfill gas (LFG) energy recover from operating and decommissioning landfills were examined. LFG energy recover is already a reality in several developed and developing countries. Here, in order to improve energetic performance of the electricity generation, hybridization of LFG with other landfill-readily available energy sources, namely solar thermal and syngas from waste gasification, are explored. The arrangement tested comprised of Integrated Solar Combined Cycle System. Several scenarios were tested with different configurations and operational modes. Results have shown that hybridization LFG powered gas turbine (GT) with solar energy in combined cycle arrangement made possible to more than doubled system power rating when compared to GT alone. However, power generation would not raise proportionally if there is limitation to solar field size, which may be the case for landfills. The addition of a supplementary of landfill-readily available energy source, such as syngas from waste gasification, compensate for this drawback and might be best option for landfill power generation or combined heat and power.

Key Words: LFG power system; Hybridization; Concentrated Solar Power; Waste Gasification

Introduction

It is well accepted that moving toward a more renewable energy matrix is a major challenge to our modern society in order to reduce green-house gas emissions from fossil-fuel based power generation. Furthermore, this same society produces large quantities of waste that holds substantial amounts of energy. Recognizing this, several initiatives to recover energy stored in waste deposition sites, such as landfill, were put in place by public and private sectors (Chen and Greene, 2003; EPA, 2016a; European Commission, 2017, 2016).

There are several technologies for energy recover from solid waste. Waste Incineration (WI), not without controversy as some Non-Governmental Organizations (NGO) claim it could potentially emit hazardous materials, is considered favorable provided that recycling is not hampered and flue gas temperature reach at least 850^{o}C (DEFRA - Department for Environment Food & Rural, 2014; European Commission, 2017; Sadi and Arabkoohsar, 2019a). WI is a proven technology with several operational unit worldwide (DEFRA - Department for Environment Food & Rural, 2014; European Commission, 2017). Other technology that is emerging for solid waste energy recover is advanced thermal treatment (ATT), such as gasification, as it has several potential advantages over WI including the generation of syngas, which is suited for different applications. On the other hand, the use of landfill gas (LFG) to generate power is widely accepted as highly beneficial (Ahmed et al., 2015; EPA, 2017; Willumsen, 2001). LFG is a biogas resulting from

anaerobic biodegradation of organic matter present in Municipal Solid Waste (Ahmed et al., 2015). It has a strong green house potential given that is composed of methane (~50%), which has global warming potential of 25 (EPA, 2016b), carbon dioxide (~45%) and other minor constituents (Ahmed et al., 2015). As such, if not burned, it is a major source of greenhouse gas especially in developing countries where this energy resource is not intensively explored (World Bank Group, 2004). Additionally, the combustion of LFG strongly reduces its toxicity having a positive impact on air pollution (Chen and Greene, 2003). Even though it is defensible that the best option is avoiding generation of LFG in the first place, by improving recycling and composting (Chen and Greene, 2003), this is not an option for those landfill in operation or being decommissioned. Thus, LFG energy-recover projects should be of high priority in public police for waste management (Chen and Greene, 2003). It is not a coincidence that there are more than 500 LFG energy-recover projects in US, for both power and heat generation (EPA, 2017).

Landfills are also convenient for solar energy projects for several reasons (EPA and NREL, 2013). Being located near highly populated area, they are usually close to high energy demand with relevant infrastructure, such as roads and power lines. Also, they are commonly constructed with large areas of minimal grade, important for sitting solar collectors. Additionally, these areas are offered at low-cost when compared to open space, since they are not suited for real state. As a consequence, in United States alone, at beginning of 2019, there were the 282 operational solar photovoltaic units in landfills, totaling 904.7 MW installed capacity (EPA, 2019). However, solar thermal application has been limited to a few research studies (Arabkoohsar and Sadi, 2018; Habibollahzade et al., 2018; Sadi and Arabkoohsar, 2019a, 2019b). Nonetheless, Concentrated Solar Power (CSP) has been shown to be highly appropriate for hybridization with other thermal energy sources for power generation (Behar et al., 2014; J. H. Peterseim et al., 2014; Juergen H. Peterseim et al., 2014). Therefore, this hybridization is suitable for LFG energy projects and will be explored here.

The hybrid power plant concept for LFG energy-recover proposed here is an Integrated Solar Combined Cycle System (ISCCS). In these systems, solar energy is used to provide additional high-pressure saturated steam to be superheated by gas turbine (GT) exhaust gases (Peterseim et al., 2013). Gas turbine has been the technology of choice for most LFG projects in large landfills. However, there are very few that apply combined cycle (EPA, 2017). Additionally, there are systems in operation using ISCCS principle (Brakmann et al., 2009; Neville, 2011; NREL, 2015) but they are implemented for natural gas powered turbine in thermoelectric power plants. Hence, the hybridization, is innovative in the application of mature technologies on a different context.

Materials and Methods

In this section the concepts, models and methodology will be presented. Information that is important but not relevant for the understanding of the results, discussion and conclusions will be left for the Appendix.

Hybrid LFG-CSP power concept

The use of the solar irradiation reaching the landfill is convenient because the area is not suitable for real estate or other intensive use. Several projects of solar photovoltaic power stations in landfills have been successfully implemented (EPA, 2019). However, CSP possess strong synergies with other fuel-powered system, as those for LFG energy recover, sharing major equipment (Peterseim et al., 2013). Furthermore, the use of CSP could be mutually beneficial. On one hand solar energy allows the increase the fuel-based power output, and, on the other, fuel raises solar conversion efficiency and offsets solar intermittence.

As a supplementary energy source to compensate for less-than-ideal solar irradiation and nighttime, synthesis gas (syngas) from waste gasification is proposed. This choice seems appropriate given that the excess of syngas not used by the power system could be converted into valuable chemicals and fuels (Arena, 2012; Hetland et al., 2011), making the best use of the gasification system. The specifics of the waste gasification are out of the scope of this study and will be subject of near future research activity. Hence, despite differences in the process and, consequently, equipment, the discussion and conclusions presented here could be easily extrapolated if the use of syngas is substituted by waste incineration such as the system proposed by (Sadi and Arabkoohsar, 2019a).

Fig. 1 presents schematically the hybrid power plant proposed. The system is a combined cycle, composed of a top Brayton cycle and bottoming Rankine cycle. To take full advantage of heat and temperatures achieved by the different fluids, exhaust gases from GT is used to superheat the steam and pre-heat feed water. Solar energy is responsible for high-pressure saturated steam generation via a heat transfer fluid (HTF), which has flown through the solar field (SF). Supplementary energy, needed when direct normal irradiance (*DNI*) is not enough to heat HTF to promote complete steam generation, is provided by syngas combustion at the Auxiliary Burner (AB). Moreover, it was also considered the possibility of Thermal Energy Storage (TES) system if the available landfill area supports a solar multiple greater than 1.0. The TES is not intended for long periods since there is a supplementary energy source. Rather, it is planned to compensate for solar intermittence and take advantage of higher-than-nominal *DNI*. As such, the TES here, if applicable, is supposed to be small and direct, that is, storage fluid is the same as HTF.

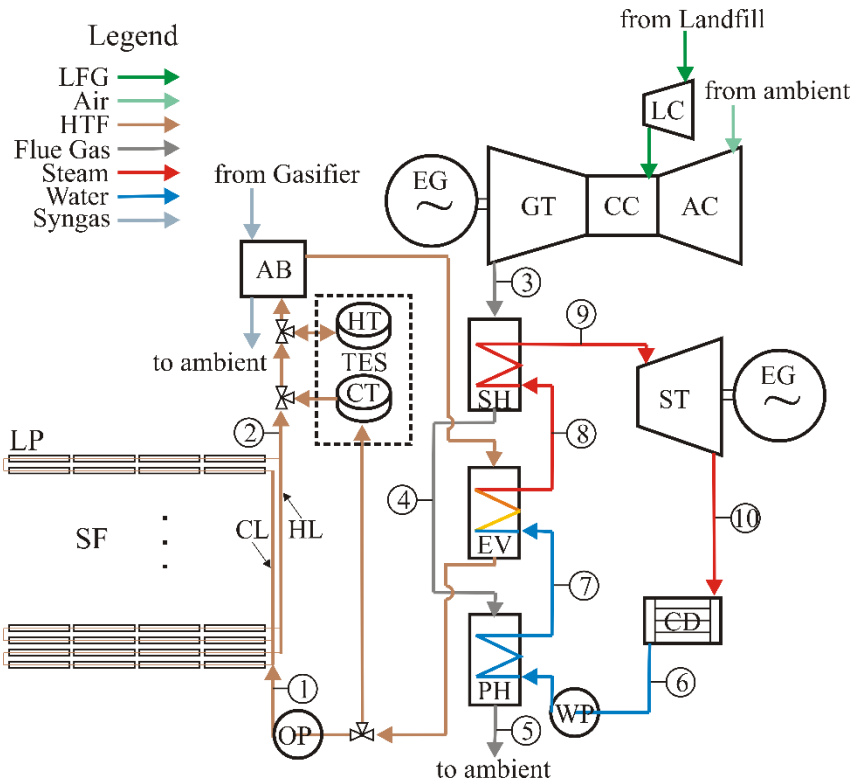

Fig. 1 Schematic diagram of the proposed hybrid plant. In the figure, the initials represent: AB-Auxiliary Burner; AC-Air Compressor; CC-Combustion Chamber; CD-Condenser; CL-HTF Cold Line; CT- HTF Cold Tank (storage system); EG-Electric Generator; EV-Evaporator; GT-Gas Turbine; HL-HTF Hot Line; HT- HTF Hot Tank (storage system); LC-LFG Compressor; LP-Linear Fresnel loop; OP-Oil Pump; PH-Pre-Heater; SF: Solar Field; SH-Super-Heater; ST-Steam Turbine; TES- HTF Thermal Energy Storage; WP-Water Pump. Numbers refer to temperature readings in Table 3.

Several scenarios with different configurations and operational modes were tested. The system shown in Fig. 1 represents the most complete one. Other scenarios were either a subset of this one or a different operational mode of it. One exception is a scenario in which the system is configured to function as Combined Heat and Power (CHP). Under this circumstance, the Rankine cycle would be composed of two steam turbines, one working as condenser turbine and the other as back-pressure.

The CSP technology of choice for this investigation was Linear Fresnel Receiver (LFR). Despite a lower optical efficiency than other current commercial CSP technologies, such as Parabolic Trough or Central Tower, LFR has some features that are relevant for the application in question. LFR, due to its simplicity, has the lowest capital investment for solar system of the same size (Morin et al., 2012), which might make it more attractive for investors given the relatively small size of the LFG power plants. Additionally, the LFR compensates for lower solar-to-thermal conversion efficiencies by allowing a denser distribution of solar modules (Morin et al., 2012). Besides that, the LFR involves less foundation work when compared to Parabolic Through (Industrial Solar, 2007) and Central Tower, the latter requiring a construction of a tall tower with a layout of heliostats (Vant-Hull, 2012) which may not be possible for the landfill area.
The solar field (SF in Fig. 1) is composed by a series of loops (LP in Fig. 1), arranged in parallel, made of LFR modules. Each loop collects HTF from the cold line (CL in Fig. 1) and delivers the heated HTF to the hot line (HL in Fig. 1). Because in most landfills, not all the area may be suitable for a CSP module installation, it was assumed that only 10% of the total area are available for the SF.

There are multiple manufacturers of commercial LFR system such as Hi-Min (Hi-Min Solar, 2020), Soltigua Solar (Soltigua Solar, 2020) and Industrial Solar (Industrial Solar, 2020). For the present study, Industrial Solar *LF-11* LFR module (Industrial Solar, 2007) was selected. This choice seemed appropriate because *LF-11* uses as absorber the evacuated tube *Schott PTR 70* (Schott Solar, 2013). Evacuated tube is a steel tube enclosed by a concentric glass tube assembled such that there is vacuum between them. *Schott PTR 70* is a high-quality state-of-the art evacuated tube that has been extensively used in Parabolic Trough power plants, the most mature of the CSP technologies (Benidir et al., 2018; Burkholder and Kutscher, 2009). Furthermore, the *LF-11* datasheet provides all the information needed to build a thermal model for system simulations (Industrial Solar, 2007). Fig. 2 shows the *LF-11* module and Table 1 presents geometric and physical properties of the *LF-11* module and the *Schott PTR 70* absorber tube.

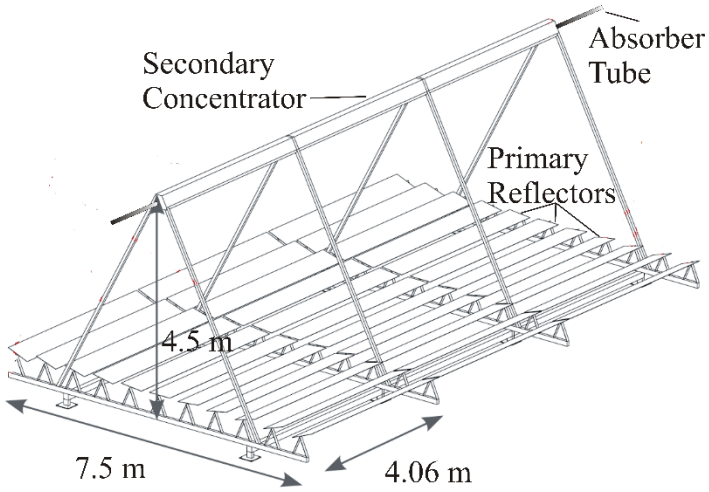

Fig. 2. LF-11 module, adapted from (Industrial Solar, 2007)

Table 1
Industrial Solar LF-11 module physical specifications

Linear Fresnel Concentrator (Industrial Solar, 2007)	
Module width	7.5 m
Module length	4.06 m
Aperture surface of primary reflectors	23 m^2
Receiver height above primary reflector	4.0 m
Height of primary reflector above ground level	0.5 m
Recommended minimum clearance between parallel rows	0.2 m
Specific weight (related to installation surface area)	26.2 kg/m^2
Maximum optical efficiency η_{max}	0.663
Evacuated Tube Absorber (Schott Solar, 2013)	
Tube length	4.06 m
Absorber outer diameter	0.07 m
Absorber SW absorptance (ISO) α_{ab}	0.955
Absorber LW Emittance ε_{ab}	0.095
Glass Envelope outer diameter	0.125 m
Glass Envelope SW transmittance τ_{ge}	0.97

Linear Fresnel thermal model

In order to estimate the solar energy harvested by the HTF at the solar field, a Linear Fresnel fully-dynamic thermal model was developed. The model solves numerically the energy balance equation for temperature of the different components of the LFR module, assembled in a loop configuration. The LFR components contemplated in the model are the HTF (*htf*), the steel absorber tube (*ab*), the glass envelope (*ge*) and secondary reflector (*sr*). Notice that there is no energy balance equation for the primary reflectors (*pr*). It was assumed that its temperature is the same as the ambient air given that it reflects most of the solar radiation.

Fig. 3 presents schematically the heat fluxes ($\dot{Q}$ in [W]) considered in the model. In order to make possible to solve the energy balance equations, the longitudinal heat fluxes were neglected, except for the HTF´s advective flux. This is a reasonable assumption given that longitudinal temperature gradients would be much smaller than transversal ones. So, the model formulation is 1-D but multidirectional. The fluxes are classified as Shortwave (solar) radiation (*SW*), Longwave (thermal) radiation (*LW*), convection (*conv*), conduction (*cond*) and advection (*adv*) assigned as the first subscript of $\dot{Q}$ in Fig. 3 and in model equations bellow. The second subscript represents the direction of the flux between the different components of the LFR. In addition to the fluxes between LFR components, there is also energy exchange between the components and the atmosphere (*atm*) and sun (*sun*).

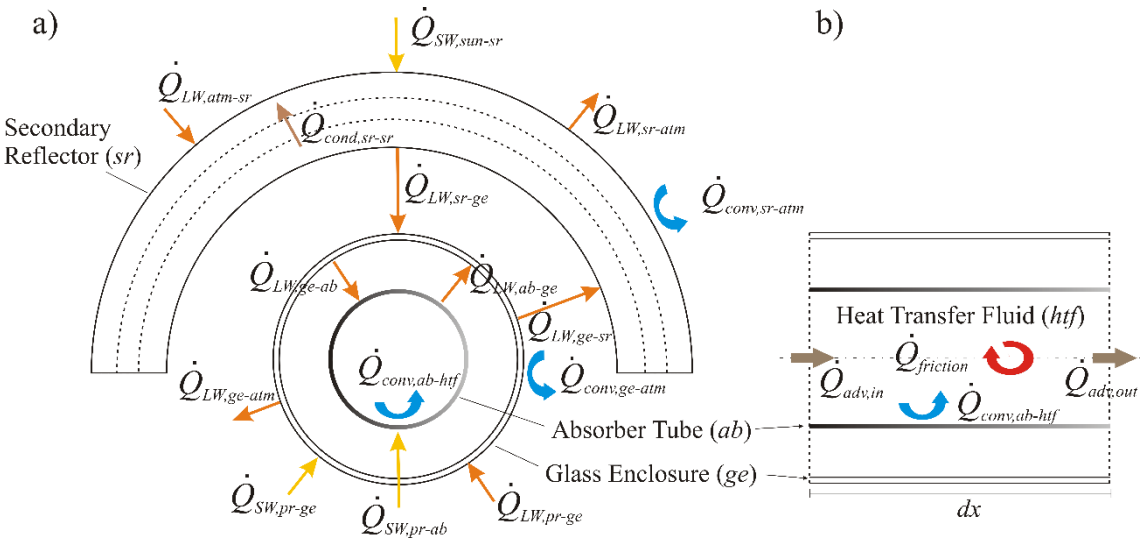

Fig. 3. Heat fluxes in the Linear Fresnel thermal model. Panel a) shows a transversal cross-section of the LFR components considered in the model. Panel b) presents a longitudinal view of control volume used to solve energy balance equation, (Secondary Reflector is omitted for clarity).

Defining a control volume as a slice of the LFR module with *dx* in length (Fig. 3b), small enough such that variables could be considered uniform, starting from the *htf*, its energy balance equation is given by:

$$\rho_{htf} c_{htf} \frac{dT_{htf}}{dt} Vol_{htf} = \dot{Q}_{conv,ab-htf} + \dot{Q}_{adv,in} - \dot{Q}_{adv,out} + \dot{Q}_{friction} \qquad (1)$$

where *T* [K] is temperature, ρ [kg/m³] and *c* [J/kg.K] are density and specific heat, respectively, *Vol* [m³] is the volume of the component within the control volume. $\dot{Q}_{friction}$ represents the oil pumping power converted in heat by friction. The advection term, present only at the HTF energy balance, is formulated as:

$$\dot{Q}_{adv,in(out)} = \dot{m}_{htf,LP} \cdot c_{htf} \cdot T_{htf,in(out)} \qquad (2)$$

$\dot{m}_{htf,LP}$ [kg/s] is the HTF mass flux within one loop. It is important to mention that the HTF temperature control, required to preserve its integrity, is achieved by varying $\dot{m}_{htf,LP}$, increasing the flux for high *DNI* and decreasing for low *DNI*, keeping the HTF close to the target temperature at loop outlet. Furthermore, the HTF removes heat from the absorber tube by convection. The convective heat flux term is modeled as:

$$\dot{Q}_{conv,ab-htf} = h_{conv,htf} \cdot A_{ab} \cdot \left(T_{ab} - T_{htf}\right) \qquad (3)$$

where A_{ab} [m²] is the internal surface area of absorber tube within the control volume, $h_{conv,htf}$ [W/m².K] is convective heat transfer coefficient. The $h_{conv,htf}$ is determined by Nusselt number defined as:

$$Nu = \frac{h_{conv} \cdot d}{k} \qquad (4)$$

where *k* [W/m.K] is the thermal conductivity and *d* [m] is a characteristic length. There are several relations for *Nu*, depending on the nature of the process, in which *Nu* is defined as a function of Reynolds, Prandtl and/or Grashof numbers. The *Nu* relations applied to the model developed here are presented at the Appendix A. However, it is worth noting that all the turbulent effects on the heat fluxes are accounted for in the *Nu* formulation, so no turbulence model is required and, consequently, momentum equation is not solved.

Considering now the absorber tube, the *ab* energy balance equation can be written as:

$$\rho_{ab} c_{ab} \frac{dT_{ab}}{dt} Vol_{ab} = \dot{Q}_{SW,pr-ab} + \dot{Q}_{LW,ge-ab} - \dot{Q}_{LW,ab-ge} - \dot{Q}_{conv,ab-htf} \qquad (5)$$

The radiative heat-flux, terms on the right-hand side of Eq. (5), are functions of the temperatures of the LFR components involved in the correspondent energy transfer. For conciseness, these formulations are provided at the Appendix A. However, it is relevant to describe here the term involving *SW* since this is where the LFR optical efficiency plays an important role. The $\dot{Q}_{SW,pr-ab}$ is given by:

$$\dot{Q}_{SW,pr-ab} = DNI \cdot \eta_{opt} \cdot A_{pr} \cdot \tau_{ge} \cdot \alpha_{ab} \qquad (6)$$

where *DNI* [W/m^2] is direct normal irradiance, A_{pr} [m^2] is the primary-reflector (*pr*) aperture area within the control volume, τ_{ge} is the glass envelope transmissivity (Table 1) and α_{ab} is absorber absorptance (Table 1). The η_{opt} is the optical efficiency of the LFR system, which, for an LFR, is a function of the longitudinal and transversal incident angles:

$$\eta_{opt} = \eta_{max} \cdot IAM_t \cdot IAM_l \qquad (7)$$

where η_{max} is the LFR maximum optical efficiency (Table 1), IAM_t and IAM_l are transversal and longitudinal incident angle modifiers, respectively. The longitudinal and transversal incident angles are dependent of solar elevation and azimuth angles. The relations between the IAM_t and IAM_l with incident angles for *LF-11* were determined experimentally by the manufacturer and are available at its datasheet (Industrial Solar, 2007). To incorporate *IAM*'s in the model, a polynomial fit applied to the manufacturers data points were used. Fig. 4 shows the behavior of the *IAM*'s as function incident angles and the polynomial forms are provided at the Appendix. Note that the IAM_l accounts mostly for the cosine effect and the IAM_t for other effects such as shadowing and blocking.

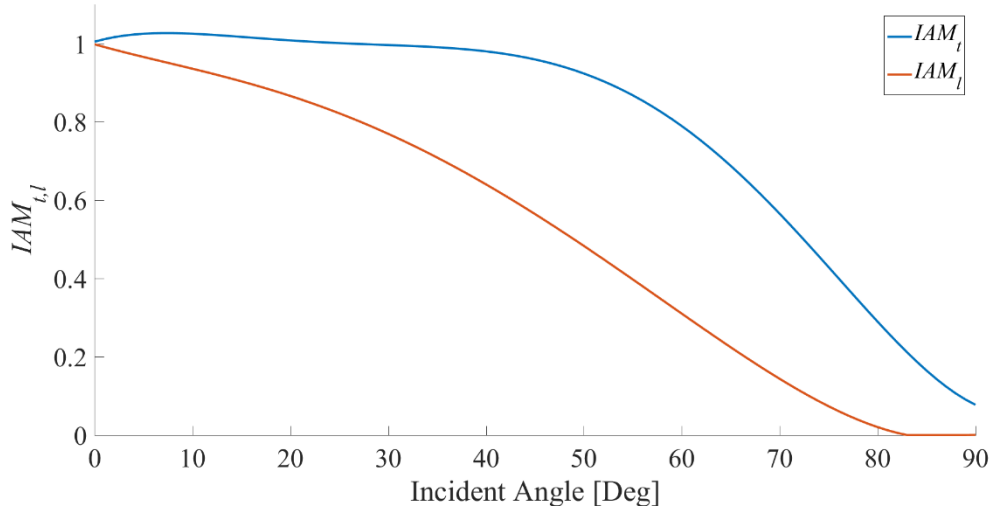

Fig. 4. Incident Angle Modifiers for LF-11 module

Another important component of the system is the glass enclosure (*ge*), its energy balance can be expressed as:

$$\rho_{ge} c_{ge} \frac{dT_{ge}}{dt} Vol_{ge} = \dot{Q}_{SW,pr-ge} + \dot{Q}_{LW,pr-ge} + \dot{Q}_{LW,sr-ge} + \dot{Q}_{LW,ab-ge} - \dot{Q}_{LW,ge-atm} - \dot{Q}_{LW,ge-sr} - \dot{Q}_{LW,ge-ab} - \dot{Q}_{conv,ge-atm} \quad (8)$$

the heat fluxes on the right-hand side are dependent on the temperatures of the components involved. Again, $\dot{Q}_{conv,ge-atm}$ are estimated by *Nu* correlation given at the Appendix. The $\dot{Q}_{SW,pr-ge}$ refers to the small portion of the *SW* that is absorbed by the glass. Note that there is no convective transfer between *ge* and *ab* given there is vacuum between them.
Finally, for the secondary reflector (*sr*), since there is an isolator between the internal and external sides, it was divided in three layers to better estimate the temperature distribution. Eq. s (9), (10) and (11) provide the energy balance for the *sr* internal, middle and external layers, respectively.

$$\rho_{sr} c_{sr} \frac{dT_{sr,int}}{dt} Vol_{sr,int} = \dot{Q}_{LW,ge-sr} - \dot{Q}_{LW,sr-ge} - \dot{Q}_{conv,sr-atm} - \dot{Q}_{cond,sr-sr,int} \quad (9)$$

$$\rho_{sr} c_{sr} \frac{dT_{sr,mid}}{dt} Vol_{sr,mid} = \dot{Q}_{cond,sr-sr,int} - \dot{Q}_{cond,sr-sr,ext} \quad (10)$$

$$\rho_{sr} c_{sr} \frac{dT_{sr,ext}}{dt} Vol_{sr,ext} = \dot{Q}_{SW,sun-sr} - \dot{Q}_{LW,atm-sr} - \dot{Q}_{LW,sr-atm} - \dot{Q}_{conv,sr-atm} + \dot{Q}_{cond,sr-sr,ext} \quad (11)$$

where $T_{sr,int}$ [K], $T_{sr,mid}$ [K] and $T_{sr,ext}$ [K] represent temperature of internal, middle and external layers, respectively. Details on each term are provided at the Appendix.
In order to find the total energy transfer to the HTF within one loop for each time step, given by the integration of $\dot{Q}_{conv,ab-htf}$ along the loop extent, the system of differential equations (Eq.s (1), (5), (8) and (9) to (11)) need to be solved for temperature of each component of the control volume. To do so, it is necessary to discretize the terms to convert it into a system of algebraic equations to be computed numerically. To the transient terms, the left-hand side of the referred equations, a forward Euler discretization is applied:

$$\frac{dT}{dt} = \frac{T_t - T_{t-\Delta t}}{\Delta t} \qquad (12)$$

where T_t [K] is the temperature at current time step, $T_{t-\Delta t}$ [K] is temperature at previous time and Δt [s] is the time step period. Additionally, fully implicit scheme was adopted, meaning that temperatures used to calculate the heat fluxes, right hand side of the equations, are taken at the current time step. For the advective term of HTF equation, Eq. (3), temperature at the control-volume longitudinal boundary is required. An "upwind" approximation was used, in which temperature at the boundary is assumed to be the same as the control volume upwind of the corresponding boundary. With this approximation, the temperatures of LFR component for each longitudinal location (control volume), arranged as a system a non-linear algebraic equation, can be calculated sequentially from the beginning to the end of LFR loop for each time step. For numerical consistency, time step period was dynamically assigned based on $\dot{m}_{htf,LP}$, which is variable depending on *DNI*, such that no HTF fluid parcel would cross over beyond one control volume during the time step. This fully-dynamic model was used here to calculate total energy absorbed by the HTF within the loop and T_{htf} at loop outlet for each time step.

To perform the model calculations, the loop size, HTF temperature at loop inlet and target temperature at loop outlet must be supplied. To do so, preliminary simulations using the System Advisory Model (SAM) platform (NREL, 2014) were carried out. SAM is a performance and financial model designed to facilitate decision making for people involved in the renewable energy industry (NREL, 2014). Even though, SAM current version allows simulations for other renewable energy concepts, it was originally conceived for CSP and it has in its database commonly used parameters for CSP applications. However, it is not appropriate for hybrid dynamical calculations needed for the purpose of this study.

With the loop configuration settled, the fully-dynamic model was executed for a typical meteorological year (TMY), the same used by SAM. During daylight, $\dot{m}_{htf,LP}$ is controlled between minimum and maximum value such that HTF temperature at outlet is maintained close the target. The TMY consisted of hourly data for *DNI*, Global Horizontal Irradiance (*GHI*), ambient air temperature and relative humidity and wind speed. Since model time steps could be shorter than one hour, a linear interpolation between hourly values of TMY were used to drive the model. This was considered appropriate given that thermal inertia of the system would filter out high-frequency oscillation of solar radiation variables in the physical system.

Thermal Energy Storage system (TES) model

As mention before, in order to take full advantage of the SF, if the landfill area available for CSP supports a solar multiple greater than one, a Thermal Energy Storage (TES, Fig. 1) is proposed. To include the TES in the LFR thermal model, the energy and mass balance equations for the Hot Tank (HT, Fig. 1) is included to consider its charging and discharging cycles:

$$\frac{dm_{htf,HT}}{dt} = \left(\dot{m}_{htf,SF} - \dot{m}_{htf,PS}\right) \qquad (13)$$

$$\frac{d\left(m_{htf,HT}\cdot u_{htf,HT}\right)}{dt}=c_{htf}\cdot\left(\dot{m}_{htf,SF}-\dot{m}_{htf,PS}\right)\cdot\left[\,f_{TES}\cdot T_{htf,SF}+\left(1-f_{TES}\right)\cdot T_{htf,HT}\,\right]-\dot{Q}_{loss,HT} \qquad (14)$$

where $m_{htf,HT}$ [kg] and $T_{htf,HT}$ [K] are mass and temperature of the HTF in the HT, respectively, $T_{htf,SF}$ [K] is the HTF temperature at SF outlet (estimated from LFR thermal model) , $u_{htf,HT}$ [J/kg] is the specific internal energy of the HTF (function of $T_{htf,HT}$, see Appendix), $\dot{m}_{htf,PS}$ [kg/s] is the HTF mass flux in the power system, which is constant, and $\dot{m}_{htf,SF}$ [kg/s] is the mass flux within the solar field. The latter varies due to HTF temperature control in the LFR loop and is given by:

$$\dot{m}_{htf,SF}=n_{loop}\cdot\dot{m}_{htf,LP} \qquad (15)$$

where the n_{loop} is the number of loops of the solar field. f_{TES} is a flag indicating if HT is being charged or discharged:

$$f_{TES}=\begin{cases}1 \text{ if } \dot{m}_{htf,SF}\geq\dot{m}_{htf,PS}\ \&\ m_{htf,HT}<m_{HT,full} \ \text{(Charging)}\\ 0 \text{ if } \dot{m}_{htf,SF}<\dot{m}_{htf,PS}\ \&\ m_{htf,HT}>0 \quad \text{(Descharging)}\end{cases} \qquad (16)$$

The value of $m_{htf,HT}$ is limited between 0 and the full capacity ($m_{HT,full}$). If Eq. (13) leads to values beyond these boundaries the solution is dismissed. $\dot{Q}_{loss,HT}$ accounts for the heat loss through the walls of the tank:

$$\dot{Q}_{loss,HT}=K\cdot A_{HT}\cdot\left(T_{htf,HT}-T_{air}\right) \qquad (17)$$

where *K* [W/m^2.K] is the loss coefficient from HT, A_{HT} [m^2] is the surface area of the HT and T_{air} [K] is the ambient air temperature. The solution of Eq.'s (13) and (14), solved numerically, provides the values for HTF conditions at the AB inlet.

Auxiliary Burner (AB) heat exchanger model

An auxiliary burner (AB, Fig. 1) is added to the system to compensate for less-than-ideal *DNI* fueled by syngas produced from a waste gasification system. The burner considered for this application is one similar to Sigma Thermal HC2 (Sigma Thermal, 2019). Note that, even though the $\dot{m}_{htf,SF}$ is variable, the mass flux in the power system ($\dot{m}_{htf,PS}$) is constant. Any mismatch between the $\dot{m}_{htf,SF}$ and $\dot{m}_{htf,PS}$ is compensated by charging or discharging HT, or extra supply from the Cold Tank (CT, Fig. 1). To keep the AB close to burners design point, it was conceived to have three burners in series deployed sequentially as a function of HTF temperature entering AB.

In order to estimate the amount of syngas consumed, AB is modeled as a heat exchanger through the Logarithm Mean Temperature Difference (LMTD) method. It was considered that the heat-exchanger global heat transfer coefficient (times area, *UA* [W/K]) remains unchanged at partial load. This approximation is justifiable by the fact that, at the oil side, the mass flux is constant so the convective heat transfer should also be and, at the gas side, although syngas mass flux is variable, the main heat transfer mechanism is radiation, which should not be

affected by changes in syngas flux. According to LMTD method applied to the AB, the heat exchange between the fluids ($\dot{Q}_{AB}$) is given by:

$$\dot{Q}_{AB} = UA \frac{\left(T_{gas,out} - T_{htf,AB,in}\right) - \left(T_{flame} - T_{htf,AB,out}\right)}{\ln\left[\left(T_{gas,out} - T_{htf,AB,in}\right) / \left(T_{flame} - T_{htf,AB,out}\right)\right]} \qquad (18)$$

where $T_{gas,out}$ [K] is the temperature of the gas exhaust from AB, $T_{htf,AB,in}$ [K] and $T_{htf,AB,out}$ [K] are temperatures of HTF entering and exiting the AB, respectively, and T_{flame} [K] is the syngas adiabatic flame temperature. Additional equations come from energy balance for each fluid and the burner nominal efficiency,

$$\dot{Q}_{AB} = \dot{m}_{htf,PS} \cdot c_{htf} \cdot \left(T_{htf,AB,out} - T_{htf,AB,in}\right) \quad (19)$$

$$\dot{Q}_{AB} = \dot{m}_{syngas} \left\{ LHV_{syngas} + c_{p,air} \left[stc \cdot T_{air} - \left(1 + stc\right) T_{gas,out} \right] \right\} \qquad (20)$$

$$\dot{Q}_{AB} = \eta_{AB,nom} \cdot \dot{m}_{syngas} \cdot LHV_{syngas} \quad (21)$$

where $\dot{m}_{htf,PS}$ [kg/s] is the HTF flux through power system, which is the same as in the AB , $\dot{m}_{syngas}$ [kg/s] is the syngas mass flux and *LHV* [J/kg] is its lower heating value, *stc* is the stoichiometric ratio for the syngas, T_{air} [K] and $c_{p,air}$ [J/kg.K] are air temperature and constant-pressure specific heat, respectively, and $\eta_{AB,nom}$ is the nominal efficiency of the burner. Characteristics of the syngas is provided in Table 1. The four equations, Eq.s (18) to (21), can be solved for *UA*, $\dot{Q}_{AB}$, $\dot{m}_{syngas}$ and $T_{gas,out}$ provided that others variables are given, which is the case for nominal values. With *UA* known, the same equations can be used to estimate $\dot{m}_{syngas}$ (and $\dot{Q}_{AB}$, η_{AB} and $T_{gas,out}$) at off-design conditions, as a function of $T_{htf,AB,in}$, which can be estimated from HTF enthalpy entering the AB (this relation is given at the Appendix). The enthalpy is calculated by Eq. (22) if the HT is being charged or discharge, or Eq. (23) if the HT is not participating:

$$h_{htf,AB,in} = \frac{\left[f_{TES} \cdot \dot{m}_{htf,PS} + \left(1 - f_{TES}\right) \cdot \dot{m}_{htf,SF} \right] \cdot h_{htf,SF} + \left(1 - f_{TES}\right) \cdot \left(\dot{m}_{htf,PS} - \dot{m}_{htf,SF}\right) \cdot h_{htf,HT}}{\dot{m}_{htf,PS}} \qquad (22)$$

$$h_{htf,AB,in} = \frac{\dot{m}_{htf,SF} \cdot h_{htf,SF} + \left(\dot{m}_{htf,PS} - \dot{m}_{htf,SF}\right) \cdot h_{htf,CT}}{\dot{m}_{htf,PS}} \qquad (23)$$

where $h_{htf,AB,in}$, $h_{htf,SF}$, $h_{htf,HT}$ and $h_{htf,CT}$ [J/kg] are HTF specific enthalpies entering AB, exiting SF, in the HT and in CT, respectively. The values calculated from its respective temperature (see Appendix). For CT, the temperature is constant as it is continuously being fed with HTF at constant temperature.

Table 2

Properties of the syngas used for this research (Hagos et al., 2014)

Property	LHV_{syngas} [J/kg]	T_{flame} [K]	stc
Syngas	17.54e6	2,385	4.58

Note: the syngas properties is referred to Syn1 in (Hagos et al., 2014), chosen because it is intermediate between the ones tested in their study.

LandGEN Model

The LandGEN model was developed by the United States Environmental Protection Agency (USEPA) to serve as a tool to estimate gas emission rates, including methane and carbon dioxide, among others, from municipal solid waste landfills (EPA, 2005). It has been extensively used in applied and research initiatives, such as the studies by Nikkhah, Khojastehpour and Abbaspour-Fard (2018), Fallahizadeh *et al.* (2019) and Sun *et al.* (2019), just to cite a few. Details of the LandGEN tool can be found at its source, EPA USA (2005a), so, here, only its main equation is presented. To estimate methane-emission rates per year, LandGEN uses the first-order decomposition rate equation:

$$W_{CH4} = \sum_{i}^{n} \sum_{j=0,1}^{1} k_{CH4} \cdot L_0 \cdot \frac{M_i}{10} \cdot e^{k_{CH4} t_{ij}} \qquad (24)$$

where W_{CH4} [m³/year], k_{CH4} [1/year] methane generation rate, L_0 [m³/Mg] potential methane generation capacity, M_i [Mg] is the mass of waste accepted in the ith year, *i* year time increment, *n* [years] is the difference between year of calculation and initial year of waste acceptance and *j* is year time increment. The USEPA provides in the LandGEN database data for k_{CH4} and L_0, which are difficult to find.

LandGEN was used to estimate the maximum extraction rate of LFG possible for a power system life cycle. To do so, it is necessary to estimate the stock of LFG as a function of time:

$$\frac{dm_{LFG}}{dt} = \rho_{LFG} \cdot \frac{W_{CH4}}{r_{CH4}} - f_{surf} \cdot m_{LFG} - \dot{m}_{LFG,PS} \qquad (25)$$

where m_{LFG} [kg] is the stock of LFG within the landfill, ρ_{LFG} [kg/m³] is the LFG density, r_{CH4} is the mixing ratio of CH_4 in LFG, here assumed 0.5 (EPA, 2005), $\dot{m}_{LFG,PS}$ is LFG mass extracted to power system and f_{surf} is a factor to account for the scape of LFG through the surface, which is considered proportional to LFG stock. Eq. (25) was solved to find the value of $\dot{m}_{LFG,PS}$ such that m_{LFG} would be zero at the end of the life cycle of the power system.

Study-case site description

In order to understand the gains in electricity generation by hybridization of landfill-readily available energy sources in an LFG-energy-recover context, the Joquei Club Brasilia (JCB) landfill was used as study case. JCB is in Brasilia, DF, the capital of Brazil. Fig. 5 shows the geographical location in the region. Also shown in Fig. 5 is the regional *DNI* distribution.

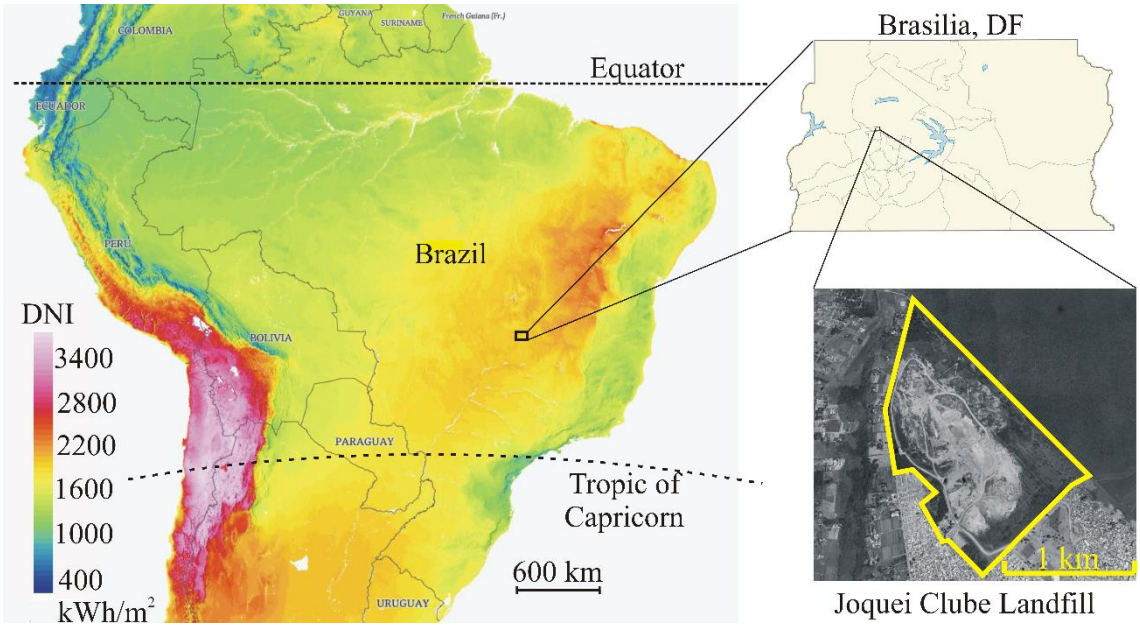

Fig. 5. Location of the study case site, Landfill Joquei Club Brasília. DNI distribution is also included in the left panel.

The landfill was stablished in 1960, the year of inauguration of Brasilia. Initially, until 1978, the waste was deposited southeast of JCB in the open in trenches, using the "ramp method", in which the soil removed for opening a cell was used to cover the adjacent one already used. From 1978 to 1995 the deposition extended in the NE and SW directions from landfill center, being considered its intermediate portion. The waste was deposited in ditches 20 to 30 m wide, 100 to 80 m long and 2 to 3 m deep. In early 1995, the disposal at the JCB covered the entire intermediate area, with the deposition being extended towards the northern portion of the landfill (Carneiro, 2002). From 1996 until 2019, when JCB was closed, part of the intermediate portion was used for the waste disposal through the "area method". Today, the total landfill area is 190 ha (Fig. 5), one of the largest in Latin America (Koller et al., 2014). More details of the landfill deposition can be found in Carneiro (2002) Santana and Imaña-Encinas (2004), Cavalcanti (2013), Cavalcanti *et al.* (2014).

As far as solar resource, the landfill is located in a region of *DNI* between 1,800 to 2,000 kWh/m^2 (Fig. 5), considered acceptable for CSP application. It is important to mention that, even though, the concept is applied to a specific location, landfill similar to JCB is common in under-developed and developing countries in Latin America (e.g. Cancharani, Puno, Peru), Africa (e.g. Kagiso, South Africa), Middle East (e.g. Zarqa, Jordan) and Asia (e.g. Surjine, Paquistan) with similar solar resource as well (Koller et al., 2014; World Bank Group, 2020).

Plant design consideration

Six scenarios, representing different plant configurations and operational modes, were tested in this investigation. Besides standard Brayton Cycle and Combined Cycle, four hybrid LFG-CSP were considered, all variants of Integrated Solar Combined Cycle System (ISCCS), with different operational modes. As mention before, Fig. 1 shows the most complete one. The methodology for designing and sizing the hybrid power system in Fig. 1 consisted of the following steps:
Using LandGEN model, LFG generation in JCB from the day it was open until the end of power system life cycle was estimated;

From Eq. (25), $\dot{m}_{LFG,PS}$ was determined in such a way that LFG stock m_{LFG} would be zero at the end of the power system life cycle;

With known $\dot{m}_{LFG,PS}$, a Brayton Cycle was specified, including, gas turbine (GT, Fig. 1), LFG compressor (LC, Fig. 1) and air compressor (AC, Fig. 1);

A thermodynamic model for a Brayton Cycle was used to estimate flue-gas mass flux and temperature;

The bottoming Rankine Cycle was modeled to estimate water mass flux ($\dot{m}_{steam}$ [kg/s]) such that the heat from flue gas would be sufficient to super-heat the high-pressure steam (at the SH, Fig. 1) and to pre-heat the feed-water (at the PH, Fig. 1);

From preliminary simulations using SAM, the nominal HTF mass flux within one loop ($\dot{m}_{htf,LP}$), loop-inlet temperature and target loop-outlet temperature were defined;

The number of solar field loops, n_{loop}, was specified considering the energy needed to evaporate high-pressure $\dot{m}_{steam}$ (at the EV, Fig. 1) and nominal solar energy harvested in one loop, from nominal $\dot{m}_{htf,LP}$, loop inlet temperature and target loop outlet temperature.

With the power system defined and solar field simulated with LFR thermal model, yearly electrical energy yield was estimated.

Results and Discussions

In this section, results from the application of the methodology, described previously, to JCB are presented. The outcome of LFG generation and solar field performance are discussed, and electric energy yield for different scenarios are analyzed.

LFG generation

The LandGEN model (EPA, 2005) presented above was applied to the conditions of JCB, Brasilia, DF, Brazil. It requires as input, the quantity of waste deposited and buried at the landfill. The waste deposited from 1960 to 2000 were taken from Carneiro (2002). From his data, a relationship was established between waste generated and population. So, from 2001 until 2016, this relationship was used to extrapolate the waste deposition using population data. The amount of waste deposited and buried from Carneiro (2002) data and extrapolated are provided in Appendix B. Fig. 6a shows the LFG generated for each year up to 2016, when it was supposed to be closed. Note that, even after the end of operation, LandGEN predicts that LFG would be generated at considerable rate (above 10 Gg/year) for about 30 years. Fig. 6b display the LFG stock (m_{LFG}) stored in the landfill, estimated by Eq. (25). In order to estimate the m_{LFG}, it was considered that 20% ($f_{surf} = 0.2$) of the current stock is lost by surface leakage each year. The blue solid line represents the stock without any power system, and the red dotted line considers a harvesting by the Combined-Cycle system designed to operate for 40 years. It was assumed that after the LFG harvesting begin the leakage would be cut to half, $f_{surf} = 0.1$, since it would create a negative manometric pressure (lower than atmospheric) on the site. The value of the $\dot{m}_{LFG,PS}$ harvested by the power system would be 0.88 kg/s, obtained by trial and error for a 30-years life cycle of the system. Fig. 6b reveals that such an intervention, besides the generation of electricity, would provide the extra benefit of reducing the time of high level of LFG (higher than 0.01 Tg) within the landfill in about 40 years and decrease the emissions of greenhouse gases, CO_2 and CH_4, to atmosphere after the system is installed.

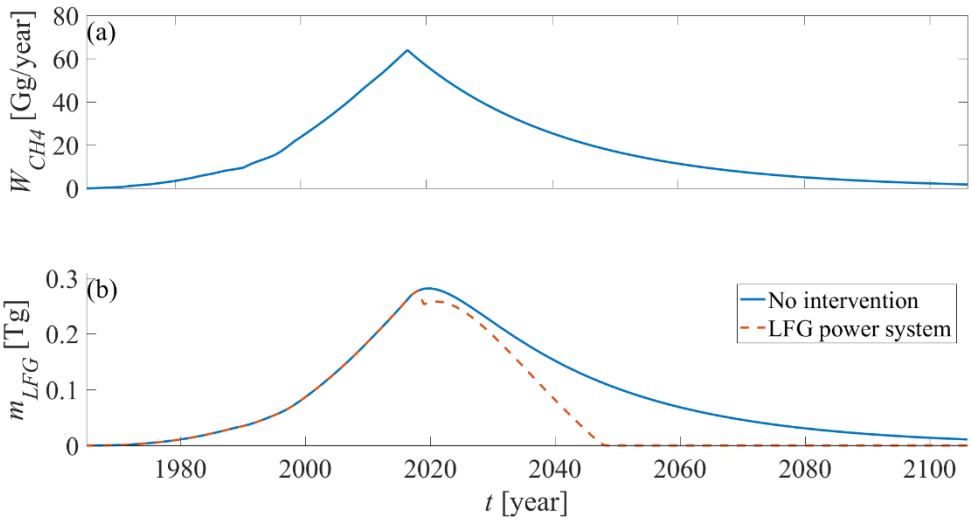

Fig. 6. LFG generated as function of time using LandGEN model (EPA, 2005), panel (a). LFG stock evolution with and without LFG power system, panel (b).

Solar system model simulation

To add confidence to the estimates of solar energy input, the LFR thermal model was validated against experimental data found in literature (Burkholder and Kutscher, 2009). The validation was focused on the heat loss, which carries out the most uncertainty. Results of the validation are presented in the Appendix. Additionally, a grid-convergence analysis was performed to make sure the results are independent of control volume size (*dx* in Fig. 3). Results for *dx* equal 1 m and 2 m were virtually the same. The results presented here are for *dx* equal 2 m.

Prior to run the model proposed here, preliminary simulations were performed using System Advisory Model (SAM, NREL (2014)). Here it was used as tool for finding an optimal solar field configuration. In this work, the thermal oil *Therminol VP1*, commonly employed for CSP applications, was used as HTF. Physical properties of *Therminol VP1* can be found on the manufacturers catalog (Eastman, 2019). Linear solar concentrators, as the Linear Fresnel, are normally designed to achieve an approximate 100-degree temperature elevation within a loop. Given the temperature limit of 400°C of the *Therminol VP1*, the temperature at the inlet was set to 290°C and the target outlet temperature to 393°C at the design operational point. This is also standard values in SAM. The length suggested by the SAM simulation was 1040 m for the *LF-11* working on *Therminol VP1*. This represents 16 modules of 16 *LF-11* collectors each, a total of 256 solar collectors, a configuration also recommended by the manufacturer (Industrial Solar, 2007). The one-loop aperture area would then be 5,632 m^2.

The solar resource in the study area, according to TMY used, would result in a total yearly direct irradiation of approximately 7,320 MJ/m^2, with a monthly distribution of daily *DNI* shown in Fig. 7. Note that, although during the period between January and March (summer) the sun is, in the average, closer to zenith, the highest values of daily direct solar irradiation happens in the period of June through August (winter). This is because, during winter, days are mostly clear (dry period) in contrast to summer days (wet period) when sky is frequently clouded.

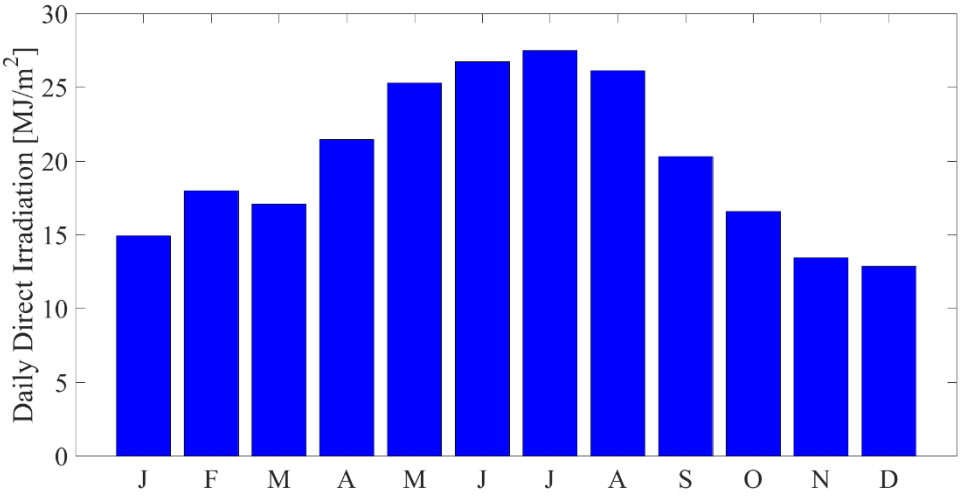

Fig. 7. Daily average direct normal irradiation for each month of the year in the study area.

The HTF temperature control, required to preserve the *Therminol VP1* integrity, was achieved by varying HTF mass flux ($\dot{m}_{htf,LP}$) within the loop, keeping the HTF close to the target temperature at loop outlet. To avoid local thermal degradation of HTF due to low advection, a minimum value for $\dot{m}_{htf,LP}$ of 3 kg/s during daytime was adopted. A maximum for $\dot{m}_{htf,LP}$ of 10 kg/s, limited by hydraulic system, was also imposed. Additionally, whenever excess of *DNI* jeopardize the integrity of HTF at the loop exit, even at the maximum $\dot{m}_{htf,LP}$, sequential LFR module defocusing of the solar field, starting from the end of loop, would be performed.

Fig. 8 shows the $\dot{m}_{htf,LP}$ for the entire year and for two typical 7-day periods, one during wet period (January) and other for the dry period (July), along with *DNI*. During wet period the $\dot{m}_{htf,LP}$ reaches higher values due to higher solar altitudes (closer to zenith during summer), which promotes higher solar-to-thermal conversion efficiency (see Fig. 4). However, the frequent presence of clouds, which drastically reduces *DNI*, makes the $\dot{m}_{htf,LP}$ at set minimum value for long periods. On the other hand, the persistent clear sky during dry period makes the $\dot{m}_{htf,LP}$ less variable and, even though the $\dot{m}_{htf,LP}$ is lower due to lower solar altitudes (winter), its consistency somewhat compensates for lower conversion efficiency. For plant dimensioning purpose, it was considered a nominal single-loop HTF mass flux of 6.5 kg/s, providing a nominal solar thermal input of 1.8 MW.

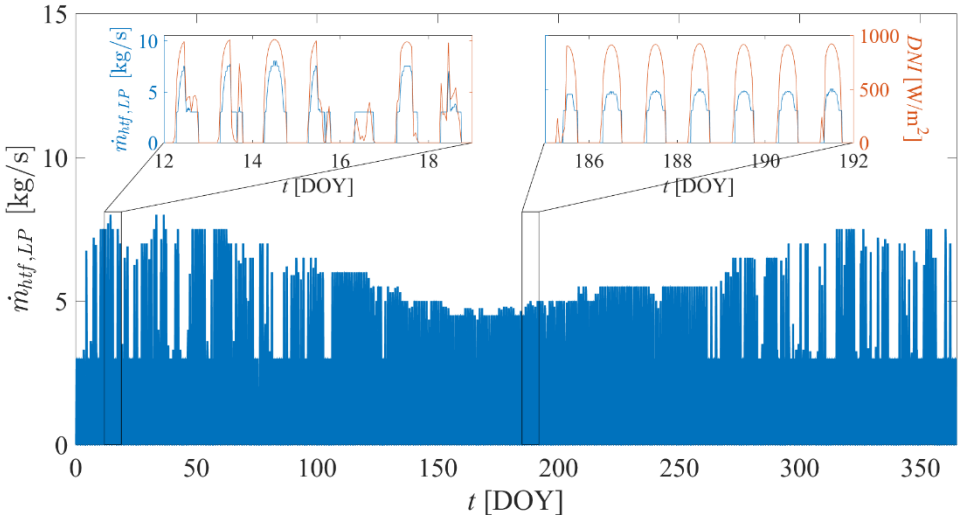

Fig. 8. HTF mass flux for the entire TMY. The insets show mass flow rate for two 7-day periods, one in January and other in July, along with the *DNI*.

Complete plant simulation

Plant configurations

Following the methodology described in section 2.6, with the LFG mass flux ($\dot{m}_{LFG,PS}$) of 0.88 kg/s estimated by LandGEN model (see section 3.2), it is possible to sustain an 8.2 MW gas turbine operating continuously for a plant life cycle of 30 years. Under these conditions, a stand-alone Brayton Cycle would have a net thermal efficiency of 31%. At the gas-turbine exhaust, the flue-gas mass flux would be 22.2 kg/s at 636°C. Adding a bottoming Rankine Cycle to make a standard Combined Cycle, these exhaust gases would support a 4.75 MW steam turbine considering an isentropic efficiency of 90%, with a steam mass flux of 3.94 kg/s, inlet temperature and pressure of 540°C and 7440 kPa, respectively, and a condensation pressure of 8 kPa. Considering the flue-gas heat input, this Rankine Cycle would have a net thermal efficiency of 36%. For this standard Combined Cycle system, the overall thermal efficiency would be 49%. Table 3 provide most relevant thermodynamic characteristics for this and all other configurations tested here and Table 4 temperature readings at the points numbered in Fig. 1.

Table 3
Thermodynamic properties of the power cycles considered in this study

Brayton Cycle		Rankine Cycle		
	GT/CC/ISCCS		CC	ISCCS
$\dot{m}_{LFG}$	0.88 kg/s	$\dot{m}_{steam}$	3.945 kg/s	11.86 kg/s
$\dot{m}_{gas}$	22.20 kg/s	P_{low}	8 kPa	8 kPa
P_{atm}	102 kPa	P_{high}	7,442 kPa	7,442 kPa
P_{comp}	1,000 kPa	η_s	0.9	0.9
$\dot{Q}_{LFG}$	26,563 kW	$\dot{Q}_{PA}$	4,370 kW	6,684 kW
$\dot{W}_{GT,gross}$	10,497 kW	$\dot{Q}_{EVA}$	5,827 kW	23,958 kW

$\dot{W}_{comp,ar}$	1,729 kW	$\dot{Q}_{SA}$	2,906 kW	8,732 kW
$\dot{W}_{comp,LFG}$	568 kW	$\dot{W}_{ST,gross}$	4,787 kW	14,385 kW
$\dot{W}_{GT,net}$	8,200 kW	$\dot{W}_{ST,net}$	4,754 kW	14,287 kW

Table 4
Temperature readings, in [°C] at the points designated in Fig. 1

Point	Fluid	Temp.	Point	Fluid	Temp.
1	HTF	290	6	Liq. Water	41
2	HTF	393	7	Liq. Water	175
3	Flue Gas	656	8	High Press. Sat Steam	290
4	Flue Gas	325	9	Super-Heated Steam	540
5	Flue Gas	70	10	Low Press. Wet Steam	41

As mentioned in section 2.1, the implementation of a Linear Fresnel SF to provide the energy for the Rankine-cycle steam evaporation (at the EV) would allow the Brayton-Cycle flue gases to be used only for superheating the vapor and preheating the feed water (see Fig. 1). Under this configuration, at *LF-11* manufacturer standard conditions of *DNI* 900W/m^2 and 30^o zenith angle (Industrial Solar, 2007), the nominal solar-to-electricity conversion efficiency would be 22%. Based on the same Brayton Cycle above, the steam mass flux can be increased to 11.86 kg/s. For the pressure of 7440 kPa of the Rankine Cycle, the evaporation energy required is 24 MW_{th}. With the maximum solar energy harvesting at one-loop of 1.8 MW (see section 3.3), 13.3 loops would be required to provide this energy. Considering the set limit of 10% of total landfill area (see section 2.6) and a packing density 0.6 (maximum suggested by the manufacturer of *LF-11* is 0.67, Industrial Solar, (2007)), a total of 20 loops could be implemented, resulting a solar multiple of approximately 1.5.
To take full advantage of the solar multiple, a small direct (storage fluid same as HTF) thermal energy storage (TES: HT and CT, Fig. 1) system is proposed. An additional benefit of TES is the damping of short-term variations of solar resource. In order to size the TES, Eq.s (13) and (14) were solved numerically for the whole year with different TES sizes. Fig. 9 shows the results of these simulations. As expected, increasing TES results in an increment yearly energy yield from solar field. However, the gain decreases as TES size increases.

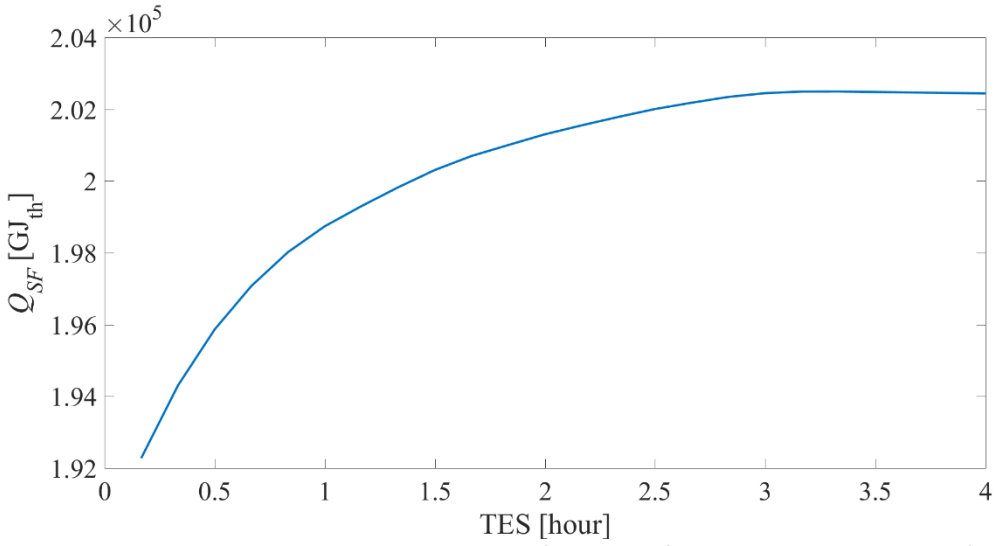

Fig. 9. Yearly energy delivered by Solar Field as a function of thermal storage system (TES)

A 1.5-hour TES resulted in a 5% increase in yearly SF energy when compared to no-TES. Above this size, energy gains would be only marginal. So, the 1.5-hour TES was chosen for yearly generation estimations. With this TES size, daily-averaged SF thermal energy for each month is presented in Fig. 10. The comparison of Fig. 10 with Fig. 7 highlights the non-linear dynamical behavior of the solar field in converting solar radiation in HTF thermal energy. The SF energy yield distribution along the months of the year is flatter when compared to *DNI* distribution. This is a result of the higher efficiency of the SF during Jan-Mar period combined with TES, which made possible the usage of the *DNI* above the limits of the power block.

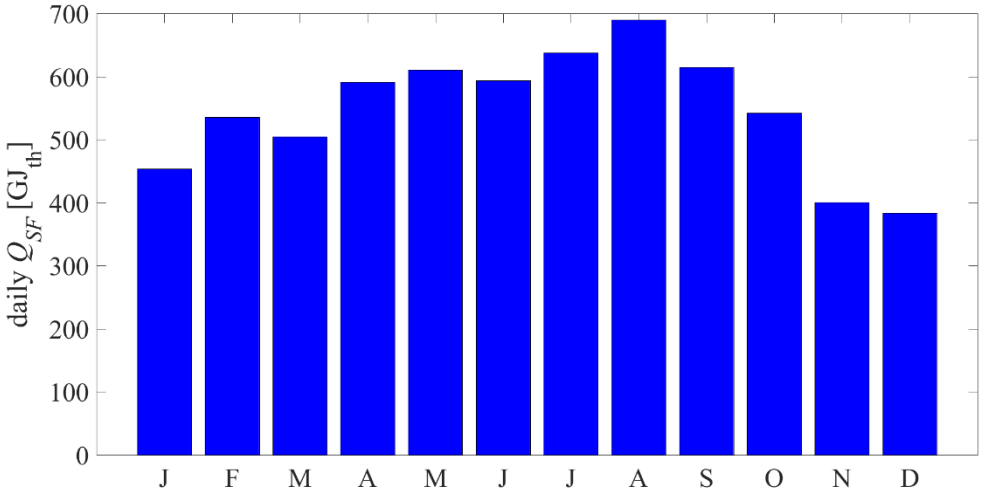

Fig. 10. Daily average SF heat to HTF for each month of the year in the study area

Yearly Electrical Energy Generation

Besides the standard Brayton and Combined Cycles, for the hybrid LFG-CSP system, four different scenarios were tested, varying system configuration and operational mode. In the first, the LFG-CSP were simulated with no supplementary source of energy as a regular Integrated Solar System Combined Cycle (ISSCC). In this case, off-design system operation must be considered. A less-than-ideal solar energy input would require a reduction of water-vapor mass flux for the Rankine cycle in order to keep a complete phase change at the EV. To take into account this effect in power output, it was considered that there would be a reduction in the isentropic efficiency of the steam turbine at partial load as proposed by Jüdes, Vigerske and Tsatsaronis (2009):

$$\frac{\eta_s}{\eta_{s,N}} = -1.0176\left(\frac{\dot{m}_{steam}}{\dot{m}_{steam,N}}\right)^4 + 2.4443\left(\frac{\dot{m}_{steam}}{\dot{m}_{steam,N}}\right)^3 - 2.1812\left(\frac{\dot{m}_{steam}}{\dot{m}_{steam,N}}\right)^2 + 1.0535\left(\frac{\dot{m}_{steam}}{\dot{m}_{steam,N}}\right) + 0.701 \quad (26)$$

Using Eq. (26), it is possible to construct a polynomial relation between power output from Rankine cycle and thermal energy from SF, Eq. (27):

$$\dot{W}_{R,pl} = -2.63\cdot10^{-6}\dot{Q}_{SF}{}^2 + 0.760\,\dot{Q}_{SF} - 2.28\cdot10^3 \quad (27)$$

In a second operation mode, syngas from waste gasification would compensate for lower-than-ideal solar irradiation making possible to run the power plant at design point continuously, referred as ISCCS+Syngas. In order to estimate the amount of syngas needed for each time step, the AB model described earlier was used to build a relationship between HTF temperature at the SF outlet, $T_{htf,SF}$, and syngas mass flux, $\dot{m}_{syngas}$, Eq. (28):

$$\dot{m}_{syngas} = -1.016\cdot10^{-5}T_{htf,SF}{}^2 - 2.7\cdot10^{-3}T_{htf,SF} + 2.65 \quad (28)$$

The response is close to linear, with thermal efficiency of AB between 88% e 91%. Eq. (28) was used to calculate the amount of syngas needed for the whole year.
An alternative mode of ISCCS+Syngas is to operate the system during daytime only, referred as ISCCS+Syngas daytime in Table 5, and keep only the standard Combined Cycle at night, similar to proposed by Sadi and Arabkoohsar (2019). This option could be advantageous for location in which tariff structure privileges high demand period, which is likely to happen during daylight, especially for workdays. In this simulations, daytime period was considered between 7:00am to 7:00pm.
Finally, another interesting option, as suggested by Ahmed *et al.* (2015), is use the LFG system as Combined Heat and Power (CHP). The authors performed a methodological comparison between several LFG-energy recover arrangements, including GT, ST and Reciprocating Combustion Engine (RCE), with and without CHP (CC was not part of their study). They concluded that optimal one is ST-CHP (Ahmed et al., 2015), provided that there is suitable usage for the heat. Furthermore, a common issue in most open landfill is leachate. Its treatment requires evaporation which demands low grade heat, compatible to counter-pressure steam turbine. So, it was also considered a scenario in which the Rankine Cycle would be composed of two turbines, one with a 4.75 MW (same the one proposed for standard CC) working at 8 kPa condenser pressure, and a second one with power rating of 6.6 MW, working in counter-pressure mode with exit pressure of 150 kPa. The two-turbine arrangement would make possible for the vacuum one work continuously and the counter-pressure during daytime.
Table 5 brings the yearly yield of electrical energy for all configurations and operational modes considered here, along with the syngas consumed. For this estimation, it was considered a conversion efficiency of 95% for the generator.

Table 5
Total Electrical Energy generated in a typical year

	Yearly Generation [GWh_e]			Syngas
Scenario	GT	ST	Total	[ton]
Brayton Cycle only	68.24	-	68.24	-
CC standard	68.24	39.56	107.80	-
ISCCS	68.24	53.35	121.59	-
ISCCS+Syngas	68.24	120.45	188.69	25,618
ISCCS+Syngas daytime	68.24	80.25	148.49	8,423
ISCCS+Syngas+CHP daytime	68.24	63.85	132.09	8,423

For the stand-alone GT (Brayton Cycle) total energy represents the installed electrical power working full time for whole year. Even though Reciprocating Combustion Energy can deliver higher conversion efficiency than GT, between 30 to 40% compared to 31% of the GT system simulated here, GT system have been preferred in USA and EU for system larger than 4 MW (EPA, 2017; Willumsen, 2001). This is because GT have significant economies of scale, as the cost drops when the GT size increases. However, this seems not to be enough for most of LFG site administrators in developing countries. In Brazil, for instance, to the knowledge of the authors, there is no GT systems, even though there are system with nominal power output greater than 4 MW using multiple RCE's. This may be due to modular installation, which grant the system the possibility of staggered investment and operation flexibility.
The addition of the bottoming Rankine Cycle to make a standard Combined Cycle (CC) allowed the power system to be augmented to 12.75 MW, increasing electrical energy generated in 58% when compared to the stand-alone GT. Even though this is considerable improvement and some studies has shown that steam turbine and combined cycle is suitable use in LFG power system (Bianchi et al., 2015; Kim et al., 2016; Sue, 2001), those systems have not been extensively applied to LFG energy projects. In USA for instance, up to 2017, out of 472 LFG electricity projects

only 20 include steam turbine or combined cycle, less than 5% (EPA, 2017). One possible explanation for this fact is that the elevation in capital cost for such energy increase would only generate marginal financial gains.

The incorporation of Linear Fresnel solar field for steam evaporation to make it an ISCCS, allowed the steam cycle system to be raised to 14.3 MW and boosted the complete ISCCS to 22.5 MW, almost double of the standard CC. However, even with the TES, the electrical energy generation did not follow the same trend and it was a little more than 15% higher. This fact was due to solar intermittency and nighttime, situations in which the system, besides lack of energy input, operates under off-design conditions.

A hybridization with an additional source, as synthesis gas from a gasification system, could compensate for this drawback, typical of CSP system. By doing so, the system could be operated at design point full time. As mentioned before, the choice of syngas for this purpose is justified by the fact the excess of syngas not used by the power system, could be used to produce more valuable chemicals and fuels (Arena, 2012; Hetland et al., 2011). The addition of the gasifier to the mix improved yearly electrical energy yield in 75% in relation to the standard CC and 55% in relation to the regular ISCCS with the expense of 25,618 tons of syngas per year. The amount of syngas is mostly used to keep the system running at design point during the night. Fig. 11a, show relative contribution from solar radiation and syngas under this configuration and operational mode. Note that, even for months with high solar radiation, the CSP contribution is still about a third of the syngas's. Of course, this comes from the limitation of using only 10% of the landfill area imposed here. For the whole year the contributions from each energy source are 61% from LFG, 10% from solar radiation, 29% from syngas.

If the operation of the ISCCS+syngas is restricted to daytime, leaving nighttime to the standard CC only, the energy generated would be reduced in 21%. However, the consumption of syngas would decrease to about a third, with the additional benefits of dispatching firm energy during high demand and to reduce size of the gasification system. Fig. 11b shows monthly relative contribution from solar and syngas for this operational mode. Comparing with Fig. 11a, it shows a more balanced profile between the two sources supplementary to LFG. For whole year the contribution from the three sources under this operation mode turns out to be 76% from LFG, 13% from solar and 11% from syngas.

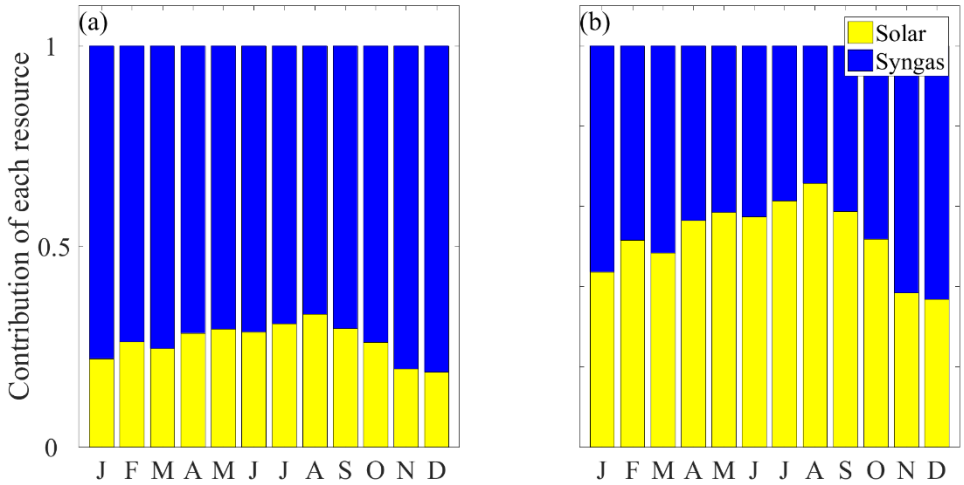

Fig. 11. Relative contribution to energy generated from solar and syngas

Least but not last, considering now the scenario ISCCS+Syngas+CHP, this configuration would reduce in 11% the yearly energy yield when compared to the ISCCS+syngas daytime. However, the heat rejection of 17.3 GW at a temperature of 111.3°C could be used in leachate treatment or other suitable uses.

Conclusions

In this study, LFG energy recover was investigated in LFG-power system context as a measure to mitigate impacts of operating and decommissioning landfills. As case study a 190ha open landfill located in Brasilia, DF, Brazil, was used. This landfill was open 1960 and operated for almost than 60 years until 2019. Several scenarios with different configuration and operational modes were considered. The scenarios include the exclusively use of LFG combustion in a gas turbine and combined cycle. Additionally, in order to improve energetic performance, hybridization with other landfill-available energy sources were tested. Here, it was considered as supplementary sources solar irradiation and syngas from waste gasification. The main findings from the study include:

LandGEN model predicted that stocked and future generated LFG would support an 8.2 MW GT for 30 years. According to previous studies, for this power rating, GT has been considered a better option than RCE (EPA, 2017; Willumsen, 2001).

The addition of bottoming Rankine Cycle to make a standard Combined Cycle improved considerably the conversion efficiency, as expected. However, according to a EPA report, combined cycle has not been the choice of most GT-powered LFG energy projects (EPA, 2017).

To take advantage of the solar resource available within the landfill area, which is not suitable for real state, a CSP solar field composed of Linear Fresnel collectors is proposed in an Integrated Solar Combined Cycle System. The CSP addition allowed the installed system power to be almost doubled. Despite the considerable increment in the power-rating, the generated electrical energy increased only 15%, due to solar intermittency and nighttime, compromising the capacity factor.

The inclusion of a third energy source, syngas from waste gasification, allowed the system to operated full load all time, with the best energetic performance at the expense of a considerable use of syngas, which may require an oversized gasification system. To avoid this problem, an operational mode in which the CSP and gasifier would work during daytime only and the system reverts to standard CC at night. The syngas use would be reduced to one third with a small reduction of energy generated but at times with lower demand (nighttime).

If leachate treatment is considered for the site, an interesting option is to have the system working as CHP for the Rankine Cycle. This option was tested with one turbine working in counter-pressure mode (daytime only) and other in condensation mode (fulltime). This arrangement would represent a 11% reduction the electrical energy generation but leaving a 17.3 GW for leachate evaporation.

It is fair to say from the results presented here that supplementing the LFG energy content with other energy resource readily available in open landfill could improve energy recover as a remediation measure. Although hybridization with solar thermal system alone, which makes possible the power system to be doubled in size, seems not to be a viable option due to low capacity factor if suitable area (here limited to 10% of total landfill area) is not available. However, the addition of a third resource to compensate solar radiation intermittency allowed to take full advantage of the improved power system. Even though the numbers of energy generated presented here are valid only for JCB, there are several landfills in developing and under-developed countries in similar conditions of landfill and solar resource that could benefit of such hybridization power system proposed.

Acknowledgements

This research was funded by CEB Geração S.A. and CEB Lajeado S.A., Brazil, under ANEEL (Brazilian Agency of Electrical Energy) R&D project entitled “Hybridization of electricity energy sources as a technological alternative of environmental remediation of areas degraded by Urban Solid Waste – Case Study: Controlled Joquei Clube landfill (Lixão da Estrutural – Brasília).

Appendix

Appendix A

For completeness, additional equations required by the LFR thermal model formulation, Eq.s (1) to (11), is provided here. Starting from heat transfer by radiation between components of the LFR, the longwave terms are given by:

$$\dot{Q}_{LW,ab-ge} = \varepsilon_{ab} \cdot A_{ab,ext} \cdot f_{ab-ge} \cdot \sigma_{sb} \cdot T_{ab}^{\ 4} \quad \text{(A1)}$$

$$\dot{Q}_{LW,ge-ab} = \varepsilon_{ge} \cdot A_{ge,int} \cdot f_{ge-ab} \cdot \sigma_{sb} \cdot T_{ge}^{\ 4} \quad \text{(A2)}$$

$$\dot{Q}_{LW,ge-sr} = \varepsilon_{ge} \cdot A_{ge,ext} \cdot f_{ge-sr} \cdot \sigma_{sb} \cdot T_{ge}^{\ 4} \quad \text{(A3)}$$

$$\dot{Q}_{LW,pr-ge} = \varepsilon_{pr} \cdot A_{pr} \cdot f_{pr-ge} \cdot \sigma_{sb} \cdot T_{air}^{\ 4} \quad \text{(A4)}$$

$$\dot{Q}_{LW,ge-atm} = \varepsilon_{ge} \cdot A_{ge,ext} \cdot f_{ge-atm} \cdot \sigma_{sb} \cdot T_{ge}^{\ 4} \quad \text{(A5)}$$

$$\dot{Q}_{LW,sr-ge} = \varepsilon_{sr} \cdot A_{sr,int} \cdot f_{sr-ge} \cdot \sigma_{sb} \cdot T_{sr}^{\ 4} \quad \text{(A6)}$$

$$\dot{Q}_{LW,sr-atm} = \varepsilon_{sr} \cdot A_{sr,ext} \cdot f_{sr-atm} \cdot \sigma_{sb} \cdot T_{sr,ext}^{\ 4} \quad \text{(A7)}$$

$$\dot{Q}_{LW,atm-sr} = LW_{sky} \cdot A_{sr,p} \quad \text{(A8)}$$

In these equations, ε, τ represent emissivity and transmittance, respectively, *A* [m²] is the emitting area, *f* is the configuration (shape) factor between the two components (Holman, 2009; Howell, 2014) and σ_{sb} is Stefan-Boltzmann constant. LW_{sky} accounts for the longwave radiation from atmosphere, which can be estimated by the Brutsaert (1975) model:

$$LW_{sky} = 1.24 \cdot \sigma_{sb} \cdot T_{air}^{\ 4} \cdot \left(\frac{e_{air}}{T_{air}} \right)^{1/7} \quad \text{(A9)}$$

where e_{air} is water-vapor partial pressure in ambient air. The remaining shortwave components are calculated by:

$$\dot{Q}_{SW,pr-ge} = DNI \cdot \eta_{opt} \cdot A_{pr} \cdot \left(1 - \tau_{ge}\right) \quad \text{(A10)}$$

$$\dot{Q}_{SW,sun-sr} = GHI \cdot A_{sr,p} \cdot \alpha_{sr} \quad \text{(A11)}$$

where *GHI* [W/m²] is Global Horizontal Irradiance, α_{sr} is the *sr* absorptance and $A_{sr,p}$ [m²] is horizontally projected area of the *sr*. Conduction term is estimated with central difference method. For instance, $\dot{Q}_{cond,sr-sr,int}$ is given by:

$$\dot{Q}_{cond,sr-sr,int} = k_{sr} \cdot A_{sr,int} \frac{T_{sr,mid} - T_{sr,int}}{dr} \quad \text{(A12)}$$

where k_{sr} [W/m.K] is thermal conduction of the isolator material in *sr* and $A_{sr,int}$ [m²] is the boundary area between internal and middle *sr* control volumes and *dr* [m] is the distance between the center of internal and middle *sr* control volumes.

Nusselt number relations required for forced convective heat flux estimation are given by (Holman, 2009):

$$Nu_{htf} = 0.23 \cdot Re^{0.8} \cdot Pr^{0.4} \quad \text{(A13)}$$

$$Nu_{ge,forc} = 0.3 + \frac{0.62 \cdot Re^{1/2} Pr^{1/3}}{\left[1 + \left(\frac{0.4}{Pr}\right)^{2/3}\right]^{1/4}} \left[1 + \left(\frac{Re}{282,000}\right)^{1/2}\right] \quad \text{(A14)}$$

In case of natural convection, convective heat transfer coefficients are directly estimated by the following (Holman, 2009):

$$h_{ge,lam} = 1.32 \cdot \left(\frac{T_{ge} - T_{air}}{dx} \right)^{1/4} \quad \text{(A15)}$$

$$h_{ge,turb} = 1.24 \cdot \left(T_{ge} - T_{air} \right)^{1/3} \quad \text{(A16)}$$

$$h_{sr,lam} = 1.32 \cdot \left(\frac{T_{ge} - T_{air}}{dx} \right)^{1/4} \quad \text{(A17)}$$

$$h_{sr,turb} = 1.43 \cdot \left(T_{sr} - T_{air} \right)^{1/3} \quad \text{(A18)}$$

where the subscript *lam* and *turb* stands for laminar or turbulent flow conditions, respectively. Additionally, thermodynamic properties of *Therminol VP1* are needed to estimate the behavior of the TES system. A functional relation between specific internal energy (u_{htf} [J/kg]) and enthalpy (h_{htf} [J/kg]) as function of temperature (T_{htf} [K]) can be derived:

$$u_{htf}\left(T_{htf}\right) = h_{htf}\left(T_{htf}\right) = 2.443 \cdot 10^3 \cdot T_{htf} - 847 \cdot 10^3 \quad \text{(A19)}$$

They are considered equal due to its incompressibility.

Furthermore, it is important to assure that the calculated solar-radiation harvested is trustworthy. Thus, in order to provide confidence in the thermal model, its validation is required. The highest uncertainty of the fully-dynamic LFR thermal model developed is associated to the evacuated-tube heat loss. The other components of the model were based on physical properties and specifications from manufacturer's datasheets which should have been extensively tested. However, the heat loss is an important component of the model since it dictates the performance of the solar-energy concentrator system. Recognizing this, Burkholder and Kutscher (2009) performed an experiment to provide heat-loss data for solar concentrator that use evacuated tube as absorber. In the experiment, the absorber-tube and glass-envelope temperatures were measured for prescribed heat flux from electrical resistance positioned inside the tube (Burkholder and Kutscher, 2009). The evacuated tube tested was the Schott PTR70, the same used in *LF-11* Linear Fresnel concentrator. In order to validate the heat-loss component included in the model, it was configured to work as in the Burkholder and Kutscher (2009) experiment. Fig. A1 shows the comparison between measured and modelled temperature readings for both absorber tube and glass enclosure as a function of electrical power input.

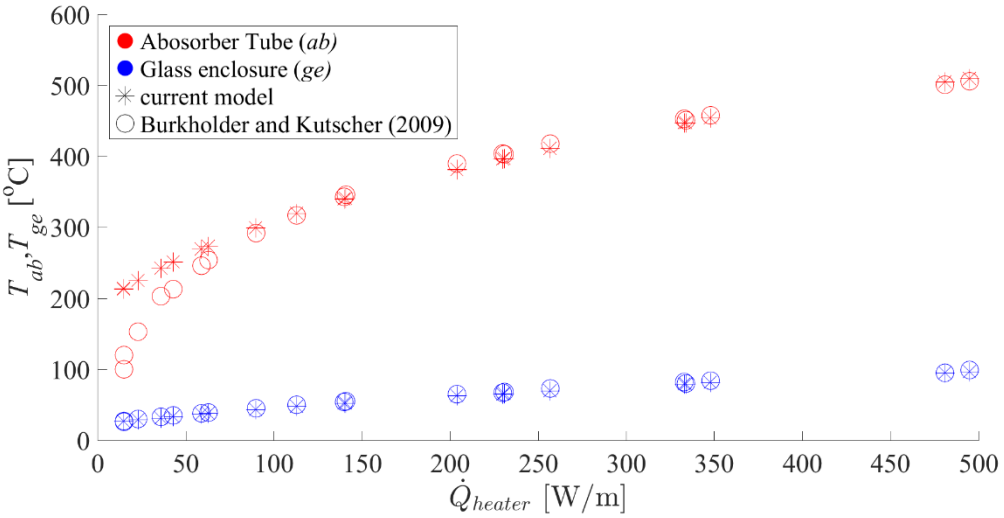

Fig. A1. Comparison between measured and modeled glass and absorber temperature as function of power input. Measured data is taken from Burkholder and Kutscher (2009)

The model tends to overestimate absorber temperature on the lower end of the power input. However, it closely follows measured results for both absorber tube and glass enclosure for power above 100 W/m and absorber temperature above 300°C. The lack of agreement for lower power range might be due to unknown ambient conditions, such as wall temperature, which might have compromised longwave-radiation exchange calculation in the model. For the higher values of input power those effects would be less relevant, and model and measurement values are virtually identical. Nevertheless, since the temperature at the solar-field inlet is already at 290°C (see section 3.3), the solar field will operate mostly at high absorber temperature, conditions at which the model performed very well in estimating the heat loss.

Appendix B

The LandGEN requires as input the amount of waste deposited at the landfill each year. From 1960 to 2000 this data is available at Carneiro (2002). Beyond that, the values were extrapolated from a relationship between population and waste generated. Table B.1 shows the value from (Carneiro, 2002) and extrapolated.

Table B.1

Waste generated and buried at JCB from 1960 until 2016

	Waste [ton]		Waste [ton]		
Year	Generated	Buried	Year	Generated	Buried
1966	16465	10674	1992	420367	306962
1967	34560	27311	1993	347372	285112
1968	38010	21244	1994	352190	298496
1969	42032	19243	1995	415037	340965
1970	58334	32354	1996	520761	444196
1971	77362	50464	1997	597230	538782
1972	92122	66982	1998	643466	581754
1973	104637	63505	1999	675090	527614
1974	102973	52625	2000	725419	560544
1975	120510	59739	2001	742844	581779
1976	146622	80115	2002	761057	603974
1977	161516	92211	2003	777597	624131
1978	172094	93157	2004	812320	666445
1979	182502	103349	2005	831536	689863
1980	191757	121032	2006	850608	713105
1981	188037	126526	2007	877750	746182
1982	206613	145146	2008	915858	792621
1983	232992	171075	2009	934573	815428
1984	212039	147703	2010	920752	798585
1985	214809	149044	2011	935745	816856
1986	256512	181986	2012	950247	834529
1987	260357	185851	2013	1003399	899303
1988	279598	149917	2014	1026963	928019
1989	293499	150168	2015	1050470	956665
1990	322975	176646	2016	1011415	967980
1991	474252	352250			

References

Ahmed, S.I., Johari, A., Hashim, H., Mat, R., Lim, J.S., Ngadi, N., Ali, A., 2015. Optimal landfill gas utilization for renewable energy production. Environ. Prog. Sustain. Energy 34, 289–296. https://doi.org/10.1002/ep.11964

Arabkoohsar, A., Sadi, M., 2018. A Hybrid Solar Concentrating-Waste Incineration Power Plant for Cost-Effective and Dispatchable Renewable Energy Production, in: 2018 IEEE 7th International Conference on Power and Energy, PECon 2018. pp. 1–6. https://doi.org/10.1109/PECON.2018.8684179

Arena, U., 2012. Process and technological aspects of municipal solid waste gasification. A review. Waste Manag. 32, 625–639. https://doi.org/10.1016/j.wasman.2011.09.025

Behar, O., Khellaf, A., Mohammedi, K., Ait-Kaci, S., 2014. A review of integrated solar combined cycle system (ISCCS) with a parabolic trough technology. Renew. Sustain. Energy Rev. https://doi.org/10.1016/j.rser.2014.07.066

Benidir, A., Khaldi, F., Benmachiche, A.H., Bouras, F., 2018. Numerical thermal analysis of schott 2008 PTR70 solar receiver under hassi R'Mel power plant operation conditions. J. Eng. Sci. Technol. 13, 122–140.

Bianchi, M., Branchini, L., Cesari, S., De Pascale, A., Melino, F., 2015. Repowering existing under-utilized WTE power plant with gas turbines. Appl. Energy 157, 902–911. https://doi.org/10.1016/j.apenergy.2015.04.076

Brakmann, G., Mohammad, F.A., Dolejsi, M., Wiemann, M., 2009. Construction of the ISCC Kuraymat, in: International SolarPACES Conference 2009. pp. 1–8.

Brutsaert, W., 1975. On a derivable formula for long-wave radiation from clear skies. Water Resour. Res. 11, 742–744. https://doi.org/10.1029/WR011i005p00742

Burkholder, F., Kutscher, C., 2009. Heat Loss Testing of Schott's 2008 PTR70 Parabolic Trough Receiver. Golden, CO (United States).

Carneiro, G., 2002. Estudo de Contaminação do Lençol Freático sob a Área do Aterro de Lixo do Jockey Club-DF e suas Adjacências. Diss. Mestr. – Univ. Brasília, Fac. Tecnol. Dep. Eng. Civ. e Ambient. University of Brasilia.

Cavalcanti, M.M., 2013. Aplicação de métodos geoelétricos nos limites do aterro aterro controlado do Jokey Club de Brasilia. University of Brasilia.

Cavalcanti, M.M., Borges, W.R., Stollberg, R., Rocha, M.P., da Cunha, L.S., Seimetz, E.X., Nogueira, P.V., de Olivera E Sousa, F.R.F.R., 2014. Levantamento geofísico (eletrorresistividade) nos limites do aterro controlado do jokey clube, vila estrutural, Brasília – DF. Geociencias 33, 144–152.

Chen, C., Greene, N., 2003. Is landfill gas green energy?

DEFRA - Department for Environment Food & Rural, 2014. Energy from waste - A guide to debate. London, UK.

Eastman, 2019. Therminol VP1 Heat Transfer Fluid.

EPA, 2019. RE-Powering America's Land Initiative: Tracking Completed Projects on Contaminated Lands, Landfills, and Mine Sites.

EPA, 2017. LFG energy project development handbook, Landfill Methane Outreach Program (LMOP).

EPA, 2016a. RE-powering America´s land initiative: renewable energy on potentially contaminated land, landfills and mine sites.

EPA, 2016b. Overview of Greenhouse Gases Greenhouse Gas (GHG) Emissions US EPA.

EPA, 2005. Landfill Gas Emissions Model (LandGEM) user's guide.

EPA, NREL, 2013. Best Practices for Siting Solar Photovoltaics on Municipal Solid Waste Landfills 41.

European Commission, 2017. The role of waste-to-energy in the circular economy. Commun. From Comm. To Eur. Parliam. Counc. Eur. Econ. Soc. Comm. Comm. Reg. COM(2017) 34 11.

European Commission, 2016. The Waste Incineration Directive - Environment - European Commission [WWW Document]. europa.eu. URL

https://ec.europa.eu/environment/archives/air/stationary/wid/legislation.htm (accessed 4.17.20).
Fallahizadeh, S., Rahmatinia, M., Mohammadi, Z., Vaezzadeh, M., Tajamiri, A., Soleimani, H., 2019. Estimation of methane gas by LandGEM model from Yasuj municipal solid waste landfill, Iran. MethodsX 6, 391–398. https://doi.org/10.1016/j.mex.2019.02.013
Habibollahzade, A., Houshfar, E., Ashjaee, M., Behzadi, A., Gholamian, E., Mehdizadeh, H., 2018. Enhanced power generation through integrated renewable energy plants: Solar chimney and waste-to-energy. Energy Convers. Manag. 166, 48–63. https://doi.org/10.1016/j.enconman.2018.04.010
Hagos, F.Y., Aziz, A.R.A., Sulaiman, S.A., 2014. Trends of syngas as a fuel in internal combustion engines. Adv. Mech. Eng. https://doi.org/10.1155/2014/401587
Hetland, J., Lynum, S., Santen, S., 2011. Sustainable energy from waste by gasification and plasma cracking, featuring safe and inert rendering of residues. Recent Exp. reclaiming energy ferrochrome from Tann. Ind. available on< www. enviroarc. com/papers. asp.
Hi-Min Solar, 2020. Fresnel Solar Receiver | Himin Coated Steel Tube | Solar Receiver Supplier [WWW Document]. URL http://himinsun.com/1-1-fresnel-solar-receiver.html (accessed 4.6.20).
Holman, J.P., 2009. Heat Transfer, McGraw-Hill Series in Mechanical Engineering. 10thed, New York, USA.
Howell, J.R., 2014. A catalog of radiation heat transfer configuration factors [WWW Document]. Univ. Austin, Texas. URL http://www.thermalradiation.net/indexCat.html (accessed 4.17.20).
Industrial Solar, 2020. Solar Thermal Collectors - Overview [WWW Document]. URL https://www.industrial-solar.de/ (accessed 4.6.20).
Industrial Solar, 2007. Fresnel Collector LF-11 datasheet. Freiburg, Germany.
Jüdes, M., Vigerske, S., Tsatsaronis, G., 2009. Optimization of the design and partial-load operation of power plants using mixed-integer nonlinear programming, in: Optimization in the Energy Industry. Springer, pp. 193–220.
Kim, M.S., Ahn, Y., Kim, B., Lee, J.I., 2016. Study on the supercritical CO2 power cycles for landfill gas firing gas turbine bottoming cycle. Energy 111, 893–909. https://doi.org/10.1016/j.energy.2016.06.014
Koller, H., Shrestha, S., Tanaka, M., Themelis, N.J., Fernando Juca, J., Pariatamby, A., Russo, M., Velis, C., 2014. Waste Atlas - The world´s biggest dumpsites - 2014 Report.
Morin, G., Dersch, J., Platzer, W., Eck, M., Häberle, A., 2012. Comparison of Linear Fresnel and Parabolic Trough Collector power plants. Sol. Energy 86, 1–12. https://doi.org/10.1016/j.solener.2011.06.020
Neville, A., 2011. Top plant: Martin next generation Solar Energy Center, Indiantown, Martin County, Florida. Power 155.
Nikkhah, A., Khojastehpour, M., Abbaspour-Fard, M.H., 2018. Hybrid landfill gas emissions modeling and life cycle assessment for determining the appropriate period to install biogas system. J. Clean. Prod. 185, 772–780. https://doi.org/10.1016/j.jclepro.2018.03.080
NREL, 2015. Concentrating Solar Power Projects by Project Name [WWW Document]. NREL. URL https://solarpaces.nrel.gov/iscc-ain-beni-mathar (accessed 4.5.20).
NREL, 2014. System advisor model, sam 2014.1. 14: General description, National Renewable Energy Laboratory,NREL.
Peterseim, Juergen H., Herr, A., Miller, S., White, S., O'Connell, D.A., 2014. Concentrating solar power/alternative fuel hybrid plants: Annual electricity potential and ideal areas in Australia. Energy 68, 698–711. https://doi.org/10.1016/j.energy.2014.02.068
Peterseim, J. H., Tadros, A., White, S., Hellwig, U., Landler, J., Galang, K., 2014. Solar tower-biomass hybrid plants – maximizing plant performance. Energy Procedia 1197–1206. https://doi.org/https://doi.org/10.1016/j.egypro.2014.03.129
Peterseim, J.H., White, S., Tadros, A., Hellwig, U., 2013. Concentrated solar power hybrid plants, which technologies are best suited for hybridisation? Renew. Energy 57, 520–532. https://doi.org/10.1016/j.renene.2013.02.014

Sadi, M., Arabkoohsar, A., 2019a. Modelling and analysis of a hybrid solar concentrating-waste incineration power plant. J. Clean. Prod. 216, 570–584. https://doi.org/10.1016/j.jclepro.2018.12.055
Sadi, M., Arabkoohsar, A., 2019b. Exergoeconomic analysis of a combined solar-waste driven power plant. Renew. Energy 141, 883–893. https://doi.org/10.1016/j.renene.2019.04.070
Santana, O.A., Imaña-Encinas, J.M., 2004. Modelo Espacial de Contaminação do Solo e do Lençol Freático do Aterro do Jockey Club para o Parque Nacional de Brasília, Brasília- DF. Cartogr. Geotécnica e Geoambiental (Conhecimento do Meio Físico) ISBN: 85-9.
Schott Solar, 2013. SCHOTT PTR ® 70 Receivers.
Sigma Thermal, 2019. Thermal Fluid System.
Soltigua Solar, 2020. Solar Tracker - Decathlon - Soltigua - PV trackers, Solar Tracker Manufacturers, parabolic trough and linear Fresnel collectors [WWW Document]. URL http://www.soltigua.com/flt-introducion/ (accessed 4.6.20).
Sue, M., 2001. A performance evaluation of combined cycle waste to energy systems (2nd report, evaluation on exergy). Nihon Kikai Gakkai Ronbunshu, B Hen/Transactions Japan Soc. Mech. Eng. Part B 67, 294–299. https://doi.org/10.1299/kikaib.67.294
Sun, W., Wang, X., DeCarolis, J.F., Barlaz, M.A., 2019. Evaluation of optimal model parameters for prediction of methane generation from selected U.S. landfills. Waste Manag. 91, 120–127. https://doi.org/10.1016/j.wasman.2019.05.004
Vant-Hull, L.L., 2012. Central tower concentrating solar power (CSP), in: Lovegrove, K., Stein, W. (Eds.), Concentrating Solar Power Technology: Principles, Developments and Applications. Woodhead Publishing, Cambridge, UK, pp. 240–281.
Willumsen, H.C., 2001. Energy recovery from landfill gas in Denmark and worldwide.
World Bank Group, 2020. Global Solar Atlas [WWW Document]. URL https://globalsolaratlas.info/map?c=-15.114553,-54.404297,4&r=BRA (accessed 3.31.20).
World Bank Group, 2004. Handbook for the Preparation of The World Bank-ESMAP Energy Sector Management Assistance Programme.